Mössbauer analysis and modeling of the order-disorder localization-delocalization transition in the mixed-valence salt diethyl biferrocenium tri-iodide

K. Boukheddaden, J. Linares, and F. Varret
Département de Recherches Physiques, Tour 22, Université Pierre et Marie Curie, 4 place Jussieu, 75252 Paris CEDEX 05, France
(Received 21 December 1992)

The thermal behavior of diethyl biferrocenium tri-iodide has been reinvestigated with further detail in the range 250–300 K by Mössbauer spectroscopy. The data strongly suggests the onset of a localized-delocalized second-order transition, and are successfully reproduced by a cooperative adaptation of the vibronic Piepho-Krausz-Schatz model. The shape and amplitude of the expected contribution to the specific heat are discussed, as well as other spectroscopic data.

I. INTRODUCTION

The mixed-valence biferrocenium cation, obtained by mono-oxidation of biferrocene, has been extensively studied (see Ref. 1 for a recent review). Concerning the intramolecular electron transfer, which is a typical feature of molecular mixed-valence salts, it soon appeared that the transfer rates and localization properties should depend on both intra- and intermolecular interactions. We have recently investigated the intramolecular aspects of electron transfer, using Piepho-Krausz-Schatz (PKS) theory, according to recent experimental data and molecular-orbital calculations.[2,9] We proposed elsewhere[3] a cooperative PKS theory, in the mean-field approximation, which leads to second-order localization transitions, in agreement with previous models based on different approaches.[4]

Such a second-order localization transition can explain the "fusion-type" behavior[5] of the Mössbauer spectra of diethyl biferrocenium tri-iodide (cation schematized in Fig. 1). At low temperature, the Mössbauer spectrum shows both Fe^{2+} and Fe^{3+} doublets. As the temperature increases, the components of the two doublets move together and at around 280 K collapse into a single "average-valence" doublet. The quadrupole splitting of this single doublet is very close to the average of splittings observed at low temperature for Fe^{2+} and Fe^{3+} moieties. Due to the absence of line broadening, it is concluded that the transfer rate is faster than the Mössbauer time scale ($\sim 10^{-8}$ s).

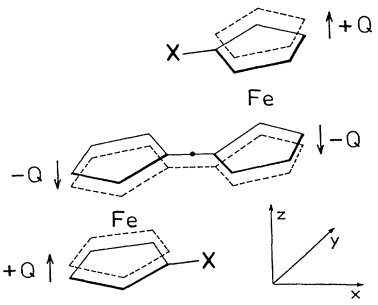

FIG. 1. Schematic view of the diethyl biferrocenium cation ($X = C_2H_5$) and its asymmetric distortion.

Using a well-crystallized sample[6] we have performed a detailed Mössbauer study in the range 260–300 K, confirming the presence of the phase transition. This is reported in Sec. II. Then we briefly recall the suitable cooperative PKS model (Sec. III) and describe the method used to calculate the quadrupole splitting within this model (Sec. IV), before discussing results in the light of specific heat and other experimental data (Sec. V).

II. MÖSSBAUER STUDY OF DIETHYL BIFERROCENIUM

We have used 120 mg of a well-crystallized sample in a 15-mm-diam sample holder. The large thickness was chosen in order to obtain good spectra statistics in the 250–300 K temperature range. Using a standard Mössbauer apparatus (25 mCi ^{57}Co:Rh, constant acceleration mode or constant velocity mode) we have performed the following.

(i) Mössbauer spectra in ± 2 mm s^{-1} velocity range every 2 degrees near the critical temperature (about 280 K, according to Nakashima *et al.*[5]). Selected spectra are shown in Fig. 2. The high-temperature spectra (283–300 K) are made of single doublets with narrow lines; the measured linewidth is temperature independent and can be considered as the experimental linewidth for the critical temperature range. The spectra below 283 K have been fitted with two symmetrical independent doublets; fitted linewidths are in excellent agreement with the experimental value quoted above. The fitted hyperfine Mössbauer parameters are reported in Table I. The measured quadrupole splittings, plotted in Fig. 6 of Sec. V, show a very fast variation in the critical range which supports the existence of a phase transition.

(ii) A thermal Mössbauer scan, at the constant velocity ± 0.90 mm/s at every degree in the same critical range (more precisely, every odd degree on increasing temperature, and every even degree on decreasing temperature). No sizable hysteresis was detected. The plot reported in Fig. 3 shows well a marked kink at 282.5 K that can be

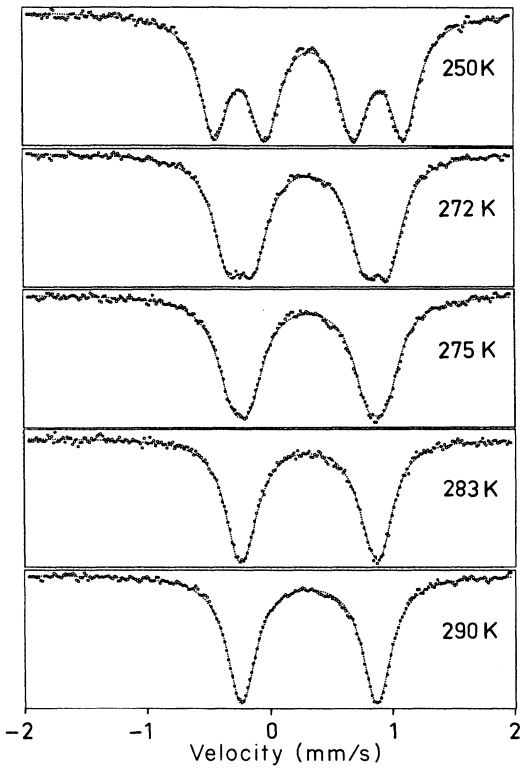

FIG. 2. Selected Mössbauer spectra in the critical temperature range.

considered as the best determination of the transition temperature in the present study.

III. COOPERATIVE PKS MODEL (AFTER REF. 3)

We start with the standard PKS model.[7] $\Psi_A(\mathbf{r})$ and $\Psi_B(\mathbf{r})$ are the basis states associated with the electron located on moiety A (Fe_A^{2+} Fe_B^{3+}) and B (Fe_A^{3+} Fe_B^{2+}), respectively. Following Piepho[8] $\Psi_{A,B}$ are identified to the highest occupied molecular orbital (HOMO's) of moieties A,B. The electronic system is coupled to an asymmetric distortion Q_- which breaks the inversion symmetry of the molecule (Fig. 1).

The vibronic basis of the problem is written as

$$\Phi_n^{\pm}=\Psi^{\pm}(\mathbf{r})\chi_n(Q_-)\ ,$$

where $\Psi^+(\mathbf{r})$ and $\Psi^-(\mathbf{r})$, respectively, are the in-phase and out-of-phase combinations of $\Psi_A(\mathbf{r})$, $\Psi_B(\mathbf{r})$ and, $\chi_n(Q_-)$ is the nth eigenfunction of the harmonic oscillator.

In this basis, the PKS elements are

$$\langle\Phi_n^{\pm}|\hat{\mathcal{H}}|\Phi_n^{\pm}\rangle=(n+\tfrac{1}{2})h\nu_-\pm J\ ,$$

$$\langle\Phi_n^{\pm}|\hat{\mathcal{H}}|\Phi_{n+1}^{\mp}\rangle=(-l/\sqrt{2})\sqrt{(h\nu_-/K)}\sqrt{n+1}\ ,$$

$$\langle\Phi_n^{\pm}|\hat{\mathcal{H}}|\Phi_n^{\mp}\rangle=W_d\ ,$$

where $Q_-=(1/\sqrt{2})(Q_A+Q_B)=2Q$, with $\pm Q$ the individual displacements of the organic rings of the biferrocenium cation (see Fig. 1), K is the elastic stiffness constant, $h\nu_-$ is the quantum of vibrational energy associated with the asymmetric distortion mode Q_- (and measured by vibrational spectroscopy), J is the transfer integral (representing the chemical bond between the moieties), l is the constant of electron vibration coupling of a moiety, and W_d is the electrostatic asymmetric potential.

The vibronic eigenfunctions obtained from the PKS Hamiltonian are written as

$$\Phi_i=\sum_n(r_{in}\Psi^+\chi_n+s_n\Psi^-\chi_n)\ . \tag{1}$$

In its static version, the PKS model provides the configuration diagram. Figure 4 shows the adiabatic energies vs the distortion parameter for the symmetric ($W_d=0$) and nonsymmetric cases ($W_d\neq 0$). According to Refs. 2 and 9, d_{xy} and d_{x-y^2} have to be considered as possible HOMO's and the vibronic electron transfer rates for the symmetric case are, for both orbitals, higher than the Mössbauer time scale ($\sim 10^8$ s^{-1}).[2] Then the symmetric case is, for Mössbauer spectroscopy, an average-valence type whatever the HOMO.

The numerical values retained here for the PKS parameters are those of the unsubstituted biferrocenium

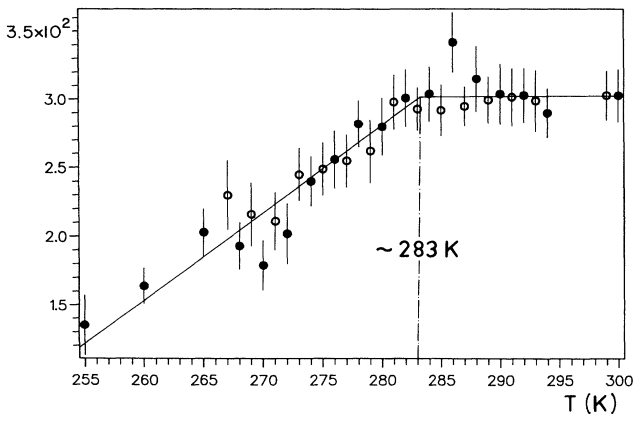

FIG. 3. Mössbauer thermal scan at constant velocity ±0.90 mm/s. The ordinate is the relative difference between the corresponding two values of the γ-ray transmission. Solid (open) circles denote data on increasing (decreasing) temperatures.

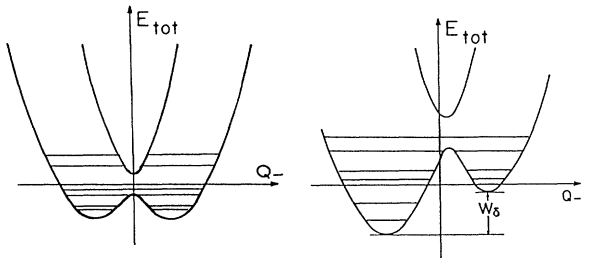

FIG. 4. Computed configurational diagrams (Born-Oppenheimer approach of the PKS model).

TABLE I. ^{57}Fe Mössbauer least-squares fitted parameters for diethyl biferrocenium tri-iodide (in mm/s), with standard statistical deviations given in parentheses.

T (K)	δ_1[a]	Γ_1	QS_1	δ_2[a]	Γ_2	QS_2
260	0.453(2)	0.286(4)	0.814(3)	0.458(2)	0.266(4)	1.494(3)
265	0.452(2)	0.296(4)	0.857(3)	0.457(2)	0.280(6)	1.442(3)
268	0.448(2)	0.302(4)	0.891(4)	0.452(1)	0.278(6)	1.415(4)
270	0.448(2)	0.308(6)	0.936(6)	0.453(2)	0.300(8)	1.364(6)
273	0.448(2)	0.306(8)	0.947(8)	0.450(2)	0.296(8)	1.320(8)
275	0.446(2)	0.316(8)	1.017(7)	0.449(3)	0.27(1)	1.325(7)
276	0.449(2)	0.324(6)	1.043(8)	0.452(3)	0.24(1)	1.314(7)
278	0.448(2)	0.312(3)	1.06(2)	0.444(2)	0.23(1)	1.28(2)
280	0.442(4)	0.312(4)	1.09(2)	0.447(3)	0.22(2)	1.25(3)
282	0.446(2)	0.310(4)	1.11(2)	0.444(5)	0.19(6)	1.27(4)
283	0.442(2)	0.310(3)	1.133(2)			
285	0.445(2)	0.300(2)	1.128(2)			
290	0.440(2)	0.290(2)	1.136(2)			
295	0.438(2)	0.306(3)	1.128(2)			
300	0.434(2)	0.298(3)	1.128(2)			

[a]The isomer shifts δ are reported with respect to metallic iron at room temperature.

cation,[2] resulting from vibrational data on ferrocene ($h\nu_-$), and MO calculations (l,J).[9]

In the solid state we must consider the interaction between molecules. So the total Hamiltonian is

$$\hat{\mathcal{H}}=\sum_i \mathcal{H}_i+\frac{1}{2}\sum_{i,j}\hat{\mathcal{H}}_{i,j} , \tag{2}$$

where $\mathcal{H}_i$ is the PKS Hamiltonian of the isolated molecule i, and $\hat{\mathcal{H}}_{ij}$ is, for simplicity, a purely electronic term represented by an asymmetric potential W_{dj} acting on molecule i.

In the mean-field approximation this potential is proportional to the quantum thermal average distortion $\langle Q_- \rangle$:

$$W_d=\eta\langle Q_- \rangle ,$$

where η accounts for both the strength and the number of intermolecular interactions around a given molecule. It is worth noting that $\langle Q_- \rangle$ is an order parameter in Landau description. Within this approach a single molecule Hamiltonian is obtained, the resolution of which requires a self-consistent method. This is performed iteratively, and $\langle Q_- \rangle$ is calculated using standard density operator techniques.

Figure 5 shows the thermal variation of $\langle Q_- \rangle$ for d_{xy} and $d_{x^2-y^2}$ orbitals, with η values chosen so as to obtain $T=280$ K as the order-disorder transition temperature.

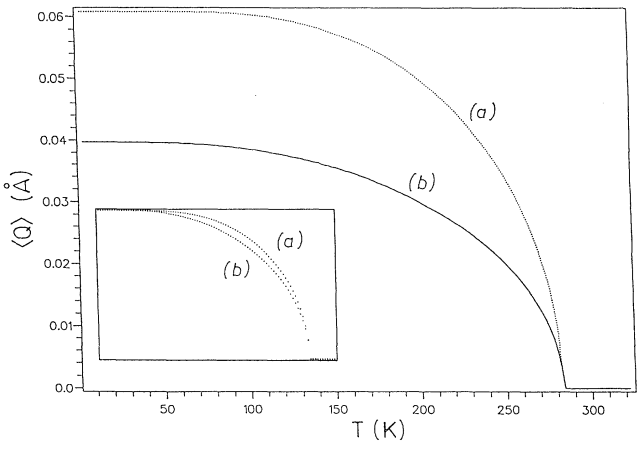

FIG. 5. Computed thermal variation of the order parameter $\langle Q_- \rangle$, leading to an order-disorder transition of second order. (a) d_{xy} (weak transfer integral $J\simeq 10.5$ cm^{-1}), (b) $d_{x^2-y^2}$ (large transfer integral $J\simeq 512$ cm^{-1}). For both, $h\nu_-=300$ cm^{-1}, $l=1.75$ eV Å^{-1}. The values of the molecular-field parameter η have been matched to obtain an order-disorder transition temperature of ~ 280 K: $\eta=0.40$, 0.76 eV Å^{-1} for (a) and (b), respectively. The inset figure shows that the shape of $\langle Q_-(T)\rangle$, in reduced scale, depends markedly on the value of the transfer integral.

IV. QUADRUPOLE SPLITTING CALCULATIONS

Due to the fast intramolecular transfer, the quadrupole splitting observable by Mössbauer spectroscopy is directly related to the probabilities P_A and P_B, having the A,B states previously defined. For a given state (energy E_i) the vibronic wave function is

$$\Phi_i=\sum_n \frac{1}{\sqrt{2}}[(r_{in}+s_{in})\Psi_A\chi_n+(r_{in}-s_{in})\Psi_B\chi_n] \tag{3}$$

and the probabilities P_A^i and P_B^i are, assuming Ψ_A,Ψ_B to be orthogonal:

$$P_A^i=\sum_n \frac{1}{2}(r_{in}+s_{in})^2 , \tag{4}$$

$$P_B^i=\sum_n \frac{1}{2}(r_{in}-s_{in})^2 , \tag{5}$$

with $P_A^i + P_B^i = 1$.

Summing up over all states, at temperature T, the total probabilities are

$$P_{A,B}(T) = \frac{\sum_i P_{A,B}^i e^{-(E_i/kT)}}{\sum_i e^{-(E_i/kT)}} , \quad (6)$$

with $P_A(T) + P_B(T) = 1$. The quadrupole splittings obtained by Mössbauer spectroscopy for iron in moieties A and B are, respectively, written as

$$QS_{\mathrm{Fe}(A)} = \alpha + \beta P_A(T) + \gamma P_A^2(T) ,$$

$$QS_{\mathrm{Fe}(B)} = \alpha + \beta P_B(T) + \gamma P_B^2(T) ,$$

where the quadratic term allows the high-temperature value to slightly differ from the average of Fe^{2+} and Fe^{3+} values. (This difference can be related to the different orientations and asymmetry parameters of the involved two EFG tensors, see Ref. 11.)

V. RESULTS AND DISCUSSION

Calculations described in this section have been performed in a vibronic space truncated to dimension 14 (seven vibrational states sufficiently span over the "active part" of the configurational diagram[2]).

From the computed temperature dependence of the order parameter $\langle Q_- \rangle$, shown in Fig. 5, it is concluded that (i) for both two orbitals, a second-order transition is obtained; (ii) the low-temperature values of the average distortion $\langle Q_- \rangle$ are sizably different for the two orbitals. However, both are in qualitative agreement with the structural data measured by x rays [~ 0.06 Å (Ref. 10)], considering the rather large uncertainties on the PKS parameters used for the present calculations; (iii) the temperature variation of $\langle Q_- \rangle$ slightly differs for the two orbitals.

The hyperfine Mössbauer parameters are reported in Table I and the quadrupole data plotted in Fig. 6. The latter have been reproduced by fitting only the parameters α, β, γ, defined in Sec. IV, and the coupling parameter η. The excellent agreement obtained with a d_{xy} HOMO, together with the lack of sensitivity of the computed curves with respect to small variations of the PKS

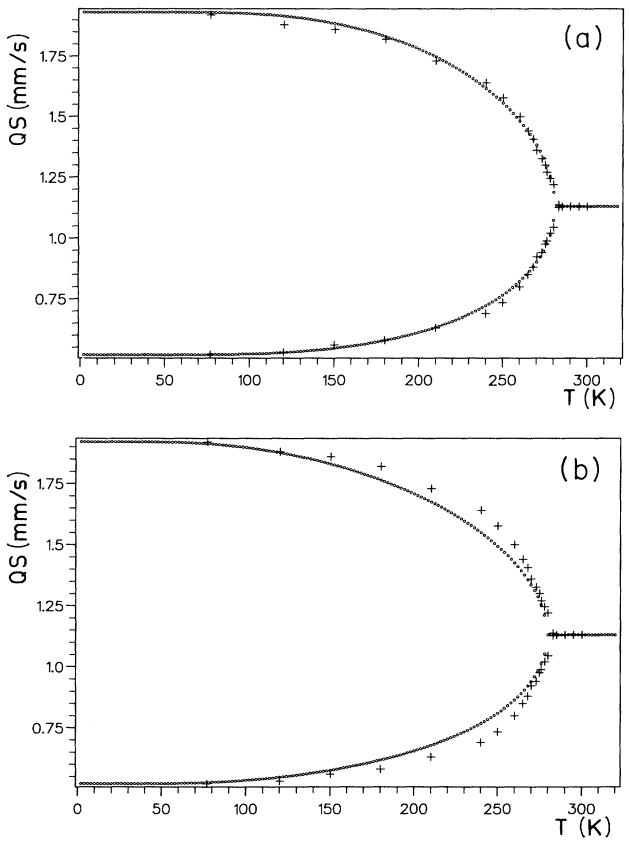

FIG. 6. Temperature dependence of the quadrupole splitting measured (+) and calculated in the frame of the cooperative PKS model (dotted line) for (a) d_{xy} orbital and (b) $d_{x^2-y^2}$ orbital.

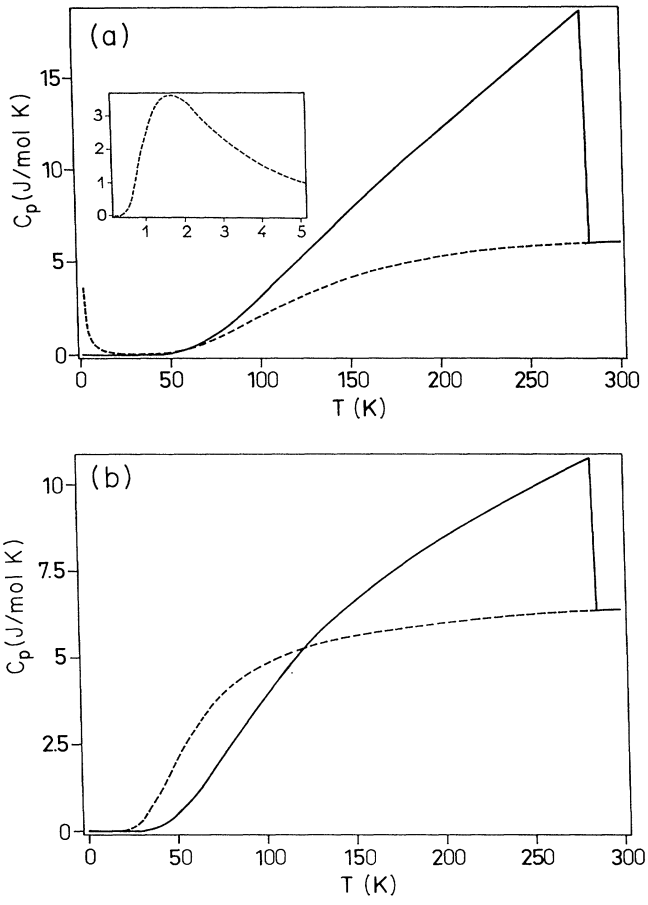

FIG. 7. Computed specific heat corresponding to the continuous transitions of Fig. 5 for (a) d_{xy} and (b) $d_{x^2-y^2}$ orbitals. The dotted lines represent the specific heat of uncoupled oscillators. A typical Schottky anomaly is shown at low temperature on the d_{xy} curve of uncoupled oscillators (inset).

parameters, dissuaded us from refining these PKS values. Thus the assumption of a d_{xy} HOMO seems to be preferred. However, this conclusion should be checked in a more general analysis involving a quasidegenerate HOMO made of both d_{xy} and $d_{x^2-y^2}$ orbitals.

Additional information may be expected from the following.

(i) Specific-heat data. We show in Fig. 7 the specific heat calculated for both orbitals in the frame of the present model. This corresponds to the contribution of the unpaired electron to the total specific heat, i.e., to the so-called "excess" specific heat in Ref. 5. Due to the difficulties from extracting the excess value from the experimental curve, only a qualitative comparison can be made; the small amplitude of the discontinuity at the order-disorder transition temperature[5] is in better agreement with a $d_{x^2-y^2}$ HOMO. However, the general shape of the experimental curve is not reproduced whatever the HOMO. On the other hand, the amplitude of the discontinuity may be decreased by the presence of short-range ordering above the order-disorder temperature. Therefore the assumption of a d_{xy} HOMO is not ruled out.

(ii) IR analysis of the C-H bending band. It has been claimed that the splitting reported for the C-H bending band near 820 cm^{-1} in diethyl biferrocenium[10(a)] above the transition temperature is associated with a double-well-shaped configurational diagram. Following Ref. 2, this should definitely favor d_{xy} as the HOMO of the system. Alternatively, $\langle Q_- \rangle = 0$ could be associated with a nonzero asymmetric potential which fluctuates at a rate between Mössbauer and IR time scales (respectively $\sim 10^8$ and $\sim 10^{13}$ s^{-1}). So far, the question remains open.

(iii) Intervalence optical band. The study of the shape and position of the intervalence band should provide useful information concerning the fluctuations of the asymmetric potential W_d. A complete interpretation might enable an independent determination of the transfer integral.

It may be expected that an extensive study of biferrocenium salts in the present framework, might lead to a more refined knowledge of the PKS parameters. Then the structural data of the molecular distortion might become conclusive concerning the choice of the orbitals.

VI. CONCLUSION

The cooperative PKS model enables us to reproduce the "fusion-type" behavior of the Mössbauer spectra of diethyl biferrocenium tri-iodide, in agreement with all available experimental data. The model concludes with a second-order transition from a low-temperature charge-ordered state to a high-temperature disordered state which is averaged at the Mössbauer time scale.

ACKNOWLEDGMENTS

We are indebted to Dr. S. Galam (GPS, University of Paris 6 and 7) for useful discussions, and to Professor H. Sano and Dr. Nakashima (Tokyo Metropolitan University) for supplying the diethyl biferrocenium tri-iodide sample. The Département de Recherches Physiques is "Unité Associée au Centre National de la Recherche Scientifique No. 71."

[1](a) H. Sano, Hyperf. Inter. **53**, 97 (1990); (b) D. N. Hendrickson, in *Mixed-Valence Systems: Applications in Chemistry, Physics and Biology, NATO Advanced Study Institute,* edited by K. Prassides (Kluwer, Dordrecht, 1991), pp. 67–90.

[2]K. Boukheddaden, J. Linares, A. Bousseksou, J. Nasser, H. Rabah, and F. Varret, Chem. Phys. **10**, 147 (1993).

[3]K. Boukheddaden, J. Linares, and F. Varret, Chem. Phys. (to be published).

[4](a) T. Kambara and N. Sasaki, J. Coord. Chem. **18**, 129 (1988); (b) S. I. Klokishner and B. S. Tsukerblat, Chem. Phys. **125**, 11 (1988); (c) A. V. Koryachenko, S. I. Klokishner, and B. S. Tsukerblat, *ibid.* **150**, 295 (1991).

[5]S. Nakashima, A. Nishimori, Y. Masuda, H. Sano, and M. Sorai, J. Phys. Chem. Solids **52**, 1169 (1991).

[6]Kindly supplied by Dr. Nakashima (Tokyo Metropolitan University).

[7]S. B. Piepho, E. R. Krausz, and P. N. Schatz, J. Am. Chem. Soc. **100**, 2996 (1978).

[8]S. B. Piepho, J. Am. Chem. Soc. **110**, 6319 (1988).

[9]F. Varret, H. Rabah, J. Guillin, and D. Talham, in *Mixed-Valence Systems: Applications in Chemistry, Physics and Biology* [Ref. 1(b)], pp. 359–364.

[10](a) M. Konno, S. Hyodo, and S. Iijima, Bull. Chem. Soc. Jpn. **55**, 2327 (1982). (b) J. A. Kramer, F. H. Herbstein, and D. N. Hendrickson, J. Am. Chem. Soc. **102**, 2293 (1980). (c) D. O. Cowan, P. Shu, E. L. Hedberg, M. Rossi, and T. J. Kistenmacher, J. Am. Chem. Soc. **101**, 1304 (1979).

[11]K. Boukheddaden, J. Linares, S. Galam, and F. Varret, J. Phys. Condens. Matter (to be published).